



CHORUS

This is the accepted manuscript made available via CHORUS. The article has been published as:

Structural transitions and metallization in dense GeS

Ranga P. Dias, Minseob Kim, and Choong-Shik Yoo

Phys. Rev. B **93**, 104107 — Published 15 March 2016

DOI: [10.1103/PhysRevB.93.104107](https://doi.org/10.1103/PhysRevB.93.104107)

Structural Transitions and Metallization in Dense GeS

Ranga P. Dias,¹⁺ Minseob Kim,² and Choong-Shik Yoo^{2*}

¹*Institute for Shock Physics and Department of Physics, Washington State University, Pullman, Washington 99164, USA;*

²*Institute for Shock Physics and Department of Chemistry, Washington State University, Pullman, Washington 99164, USA;*

+ *Currently at Lyman Laboratory of Physics, Harvard University. Cambridge, MA02138*

* *Corresponding author: csyoo@wsu.edu*

ABSTRACT

We have studied the pressure-induced structural and electronic transitions of GeS to 49 GPa, using diamond anvil cells, micro-confocal Raman spectroscopy, synchrotron angle-resolved x-ray diffraction and electrical resistance measurements. The results indicate that layered GeS phase I ($Pnma$) undergoes two structural phase transitions: first to phase II ($P2_1/m$) at ~ 9 GPa and then phase III ($Cmcm$) at ~ 32 GPa. These transitions occur sluggishly over large pressure ranges and accompany an increase of the nearest coordination number of Ge and S atoms from three in phase I and II to five in phase III, resulting in an extended network of densely packed layer structures in phase III. We suggest anisotropic-compression enhanced shears to be responsible for the transitions. The phase II also undergoes an electronic insulator-metal transition and becomes metallic above 20 GPa, The temperatures dependent resistance change of phase II further indicates a gradual band-gap closing of phase II ($P2_1/m$).

INTRODUCTION

The compounds consisting of group-IV elements (Ge, Sn) and group-VI elements (S, Se) are in many respects an interesting group of compounds. They are known as narrow-gap semiconductors or semimetals, which have potential implications for various optoelectronic applications [1-3]. At ambient pressure, those compounds adopt an orthorhombic structure with eight atoms per unit cell forming double-layer planes normal to the longest axis, which closely related to that of black phosphorous [4-6]. However, there are only a few studies on these group IV-VI systems at high pressures [7-12]. As such, the presence or absence of phase transitions in some of these compounds is still uncertain [13], resulting in incomplete understanding of the transition pathway [14-16].

It is well known that shear deformations alter the stability of phases and change the mechanism of phase transition. This is particularly evident in layer structures. Therefore, the controversies on the previous studies may be due to non-hydrostaticity of the applied pressure because the group IV-VI compounds are made up of puckered layers sensitive to shear stress [17,18]. On the other hand, the electrical resistance measurement on GeSe [19] showed monotonically decreases with increasing pressure, which was interpreted in terms of a metallization above 25GPa. The presence of metallization reflects a weakening of covalent character in Ge-Se bonds. It is also well known that the vibrational spectra of layered crystals are characterized by low frequency optical phonons [20]. They can be attributed to shear modes, where adjacent rigid layers move in parallel to each other, and compressive modes, where layers vibrate against each other.

Relatively few studies have been done on GeS at high pressures, hampering the systematic understanding of structural, vibrational and electrical properties of dense group IV monochalcogenides. GeS is the least anisotropic member of orthorhombic group IV-VI compounds and behaves as if it were an intermediate case between a two dimensional (*2D*) layered structure and a *3D* network structure. Earlier x-ray diffraction studies showed that the orthorhombic structure of GeS is stable up to 34 GPa [8]. Yet, later first principles theoretical studies predicted that GeS undergoes a gradual phase transition to an orthorhombic (*Cmcm*) phase above 34 GPa and also exhibits the metallization prior to the transformation to the *Cmcm* phase [21]. These theoretical results have yet to be confirmed experimentally.

In this paper, we present new findings of the pressure-induced structural and electronic phase transitions in GeS using micro-Raman spectroscopy, electrical resistance and synchrotron x-ray diffraction measurements.

EXPERIMENTAL METHODS

The sample was crystalline GeS (99.99% from Sigma-Aldrich). In order to obtain a fine powder sample, a single crystal sample was first crushed to fine powders then loaded onto a membrane-driven diamond-anvil cell (m-DAC), using 1/3-carat, type Ia diamond anvils with a 0.3 mm culet. A 0.2 mm thick rhenium gasket was pre-indented to 40 μm and 120 μm hole was electro-spark drilled at the center of the gasket. We used neon as a pressure transmitting medium and a few chips of ruby for pressure calibration. Care has

been taken not to bridge the sample and ruby between two diamond anvils. The Raman spectra of GeS were obtained using a home-built confocal micro-Raman system based on a Nd:YLF laser (used the 2nd harmonic at 532 nm). The samples were a modified cryostat (Cold-Edge Tech, PA) to adapt our m-DAC for simultaneous operation of Raman and electric resistance measurements down to 5 K at high pressures.

Angle-resolved x-ray scattering data were collected at room temperature using micro-focused ($\sim 10 \times 10 \mu\text{m}$) monochromatic synchrotron x-ray at 16BMD/HPCAT ($\lambda = 0.406625 \text{ \AA}$) at the Advanced Photon Source. The x-ray scattering intensities were recorded on high-resolution 2D image plates over a large 2θ range between 0 and 40 degrees and then converted to 1D profiles using the Fit2D program [22]. Rietveld refinement was then performed to determine the crystal structure using General Structure Analysis System (GSAS) program [23] with EXPGUI [24].

In electrical resistance measurements, fine alumina powders mixed with epoxy were used for the purpose of electrical insulation of four 5-mm thick platinum electrodes from metallic Re gaskets. A 40 to 60 μm hole sample chamber was drilled at the center of the insulation powder. The van der Pauw method [25] using 5 μm thick platinum electrodes was implemented with an average distance between opposite electrodes being around 30 to 35 μm . DC electrical resistance measurements were performed with 3 mA current, Lakeshore 120 current source with switching polarity, and the voltage readout from Keithley 2000 DVM was recorded on a computer. For low resistance values AC technique was used at 13 Hz frequency and 3 mA current from Stanford Research SR830

digital lock-in amplifier. The electrical resistivity was calculated through Van der Pauw's equation [25],

$$\exp[-\pi LR_A/\rho] + \exp[-\pi LR_B/\rho] = 1,$$

where $R_A = V_A/I_A$ and $R_B = V_B/I_B$ represent the resistance, ρ and L represent the resistivity and thickness of sample, respectively. The pressure-induced thickness change of the sample was determined by measuring the distance change of the back facet of two diamond anvils using a micrometer.

The low temperature electrical resistance of GeS was measured using closed-cycle refrigerator (ColdEdge-SDRK-408D), custom designed for low vibration and m-DAC. The cold head uses helium gas and consists of two physically separated stages for low vibration, providing cooling to 25-45 K at the first stage and to 3.5-4.2 K at the second. A small amount of helium (less than 0.5 psi) was introduced to fill the space between the two stages as a heat exchange gas. The coldest part of the cryostat is around 5 cm above the top of the DAC. Two thermometers were placed in the top and middle of m-DAC to measure the sample temperature.

RESULTS

A. Raman measurements

A factor-group analysis of the three dimensional space group D_{2h}^{16} reveals 24 vibrational modes [26, 27]. Their representation at the center of the Brillouin zone is $\Gamma =$

$4A_g + 2B_{1g} + 4B_{2g} + 2B_{3g} + 2A_u + 4B_{1u} + 2B_{2u} + 4B_{3u}$. Apart from three acoustic vibrations, there are 21 optical phonons: two are inactive ($2A_u$), seven are infrared active ($3B_{1u}, 3B_{3u}, 1B_{2u}$), and twelve are Raman active ($4A_g, 2B_{1g}, 4B_{2g}, 2B_{3g}$). The structure consisting of double layers (perpendicular to the c axis) are covalently bonded and forms a zigzag chain along the direction of the minor axis of the crystal in which Ge and S atoms are threefold coordinated to each other. Materials with this structure are expected to exhibit three zone center rigid-layer optical vibrations. One of the modes is a rigid-layer modes which individual layers move each other as a unit, and the other two modes are shear displacements in which the layers slide over each other by bond bending and covalent bond length changing in the a and b directions. Also the degeneracies due to layer symmetry are lifted when coupling between layers is introduced and the modes split into Raman active doublets.

The Raman spectra of GeS under hydrostatic pressure are presented in Fig. 1 and the pressure dependent shifts of the observed Raman modes in Fig. 2a. The peak positions were obtained by the spectral deconvolution of the data in Fig. 1 as illustrated in Fig. 2b. According to the previous reports [4] at ambient conditions Raman frequencies could be grouped into three lowest frequencies ($\sim 52, \sim 64$ and ~ 77 cm^{-1}), somewhat higher frequencies (ranging from ~ 88 cm^{-1} to ~ 133 cm^{-1}) and considerably higher frequencies (ranging from ~ 210 cm^{-1} to ~ 300 cm^{-1}). The lowest frequency modes occur at 111 cm^{-1} (A_g shear mode). The observed Raman modes show the increasing mode frequencies with increasing pressure as expected. However, one of the higher frequency modes (bond stretching type) at 269 cm^{-1} shows a clear discontinuity of the rate of

change of the frequency above 8 GPa from $2.949 \text{ cm}^{-1}/\text{GPa}$ to $4.176 \text{ cm}^{-1}/\text{GPa}$ (Fig. 2). Also observed was a splitting of one of the A_g modes above 8 GPa. Above 30 GPa, one new rather broad peak appeared at $\sim 331 \text{ cm}^{-1}$, indicating a structural phase transition. The Raman intensity of GeS gradually decreases roughly by a factor of 2-3 over the pressure range of 1-15 GPa, as it metallizes (which will be discussed later in section C).

B. Structural properties

Figure 3 shows angle-dispersed powder x-ray diffraction patterns of GeS as obtained at pressures up to 49 GPa. A broad background feature between $2\theta = 4^\circ$ to 16° is most likely from x-ray Compton scatterings of diamond anvils. It is notable that the number of diffraction peaks decreases significantly with increasing pressure, while the powder diffraction pattern is maintained to 49 GPa. Based on the changes in diffraction patterns, we determine two structural phase transitions; the first transition at 9 GPa by splitting of a peak centered at $2\theta \sim 11^\circ$, and the second one at 32 GPa by merging two peaks between $2\theta = 8^\circ$ to 8.5° and a triplet centered at $2\theta \sim 9-10^\circ$. The first transition at 9 GPa is consistent with the pressure where the A_g mode splits (Fig. 2). The second structural transition at 32 GPa is, however, somewhat higher than observed in Raman, 28 GPa, suggesting a sluggish nature of the transition. The spurious features marked with asterisk '*' in Fig. 3 are from a small amount of impurities such as sulfur.

The pressure dependences of d-spacings (Fig. 4) show the onsets of phase transitions, signified by the disappearance of diffraction peaks, the pressure evolution of

peak positions, and the change of peak shift-rates. In the inset, the 2D diffraction images are also presented to show evidence for lattice texture and preferred orientation in GeS polymorphs. No dramatic change of d-spacing was observed across the phase II→III transition, hinting a gradual structural phase transition.

Figure 5 presents the refined x-ray patterns of GeS polymorphs: phase I at 5 GPa for *Pnma* and phase II at 16 GPa for *P2₁/m* using the Rietveld method, and phase III at 49 GPa for *Cmcm* using the LeBail fit. The resulting structural models are illustrated in Fig. 6. Up to 9 GPa, the x-ray data fit well with an orthorhombic *Pnma* structure previously reported [4]. It shows a reasonably good Refinement result with a reduced $\chi^2=2.32$; the lattice parameters at 5 GPa are $a=10.068(1)$ Å, $b=3.605(1)$ Å, $c=4.055(1)$ Å, $\rho=4.72$ g/cm³ with $Z=4$. All Ge and S atoms are at $4c(x, 0.25, z)$ site; the refined atomic coordinates are Ge (0.386(3), 0.250, 0.088(9)) and S (0.149(6), 0.250, -0.020(1)).

The diffraction patterns between 9 and 19 GPa can be interpreted in terms of both phase I (*Pnma*) and a new phase II (*P2₁/m*) with similar R-factors. Therefore, it appears that the transition occurs rather gradually over the same pressure range. The calculated volume difference between the two structures is about ~3.5% at the transition pressure 9 GPa, which gradually decreases with increasing pressure, as shown in Fig. 7. No apparent volume difference between the two structures at 19 GPa. The low-pressure *Pnma* structure, however, fails to fit the observed data above 19 GPa, whereas the *P2₁/m* structure continues to fit well the observed diffraction patterns up to 30-40 GPa.

The refined results of phase II at 16 GPa is shown in Fig. 5. Note that the refined lattice angle in this monoclinic cell is small as a few degrees; nonetheless, it improves intensity fitting significantly and provides better descriptions for the peak merging at $2\theta = \sim 8^\circ$ and the peak splitting at $2\theta = \sim 12^\circ$. The best refinement of phase II at 16 GPa, based on the $P2_1/m$ structure with $Z=4$ yields the cell parameters of $a=9.628(2)$ Å, $b=3.506(1)$ Å, $c=3.780(2)$ Å, $\beta=90.10^\circ$, $\rho=5.430$ g/cm³ with a reduced $\chi^2=0.92$. In this structure, both Ge and S are assigned to $2e(x, 0.25, z)$ sites, and the preferred orientation is placed on the (111) plane. Comparing with phase I, the structure model of phase II (Fig. 6) shows a slight reduction in the average intralayer Ge-S distance from 2.43 Å to 2.29 Å, a small increase in the intralayer Ge-S-Ge angle from 96° to 101° , and a small decrease in the interlayer Ge-S-Ge angle from 105° to 103° . As such, in phase II the bilayer structure becomes more puckered and the next nearest neighboring S and Ge becomes closer. The detailed structure information are summarized in Table. 1.

Above 32 GPa, new phase III emerges by merging and reducing the number of multiplets. The characteristic doublet at $2\theta = \sim 8^\circ$ and triplet at $\sim 9^\circ$ for phase II merge to single peaks. The separation of two overlapping peaks at $2\theta = \sim 12.5^\circ$ become larger with increasing pressure. Most of the diffraction features can be described reasonably well in terms of an orthorhombic $Cmcm$ structure, with an exception of the peak at $2\theta = \sim 7.2^\circ$. Note that the calculated (110) peak position appears at $\sim 7.0^\circ$ with relatively weak intensity. The weak intensity is due to the puckered layer structure deviating sulfur atoms from the (110) plane. Therefore, it is considered that the 7.2° peak intensity is mainly coming from the low-pressure $P2_1/m$ phase which has not been completely transformed.

The diffraction pattern at 49 GPa in Fig. 5, therefore, has been refined based on a mixture model of a primary *Cmcm* phase III and a minor *P2₁/m* phase II. The refined cell parameters of phase III are: $a=3.624(1)$ Å, $b=9.030(10)$ Å, and $c=3.367(1)$ Å with $\chi^2 = 2.98$. The atomic coordinates are: Ge(0.0, 0.859(1), 0.25) and S(0.0, 0.592(1), 0.25). The refinement uses a preferred orientation on the (200). The same refinement also yields the lattice parameters for phase II: $a=9.2290(12)$ Å, $b=3.295(3)$ Å, $c=3.649(5)$ Å and $\beta=96.17^\circ(4)$, resulting in nearly the same volume as that of phase III. In the *Cmcm* structure of phase III, Ge (or S) connects two additional neighboring S(or Ge), forming five-fold coordinated Ge and S atoms in pyramidal polyhedral layers (Fig. 6). It is an interesting feature of phase III that the intralayer Ge-S distance is elongated from 2.29 Å to 2.51 Å and the interlayer Ge-S distance (along the *b*-direction) from 2.29 Å to 2.42 Å respectively. The increase of inter- and intra- layer Ge-S bond distances in phase III, in turn, reflects an increase of sharing electrons with a larger number of neighboring atoms (*i.e.*, 5 fold coordination) by orbital hybridization and thereby a reduced bond order.

Crystal structures of GeS polymorphs are compared in Fig. 6, showing GeS double layers stacked along the *a*-axis in phase I and II and along the *b*-axis in phase III. In phase I and II, Ge and S atoms in the layers are covalently bonded with three neighbors to form three-fold coordinates, and the layers are held by a weak van der Waals interaction at the interlayer distance of ~ 2.9 - 3.1 Å – too far to form a covalent bond. On the other hand, the interlayer distance decreases substantially in phase III; it becomes ~ 2.5 Å at 49 GPa – close enough to form covalent bonds between Ge and S atoms in adjacent layers. This results in five-fold coordinated Ge and S atoms in phase III. This is in contrast to the

nearest Ge-S distances within the layers remain nearly same at 2.3-2.5 Å for all three phases. Therefore, it is likely that the phase II → III transition is driven by anisotropic compression of the layered structure, resulting in the formation of additional Ge-S bonds between two adjacent layers. This conjecture is in fact supported by strong compressibility observed along the c-axis in phase I and II (Figs. 7 and 8). Recall that the II → III transition occurs over a large pressure range without any discontinuous volume change. In fact, the remnant of phase II is present even at 49 GPa. This further indicates the transition is driven by the enhanced shear stress developed between the layers of phase II. The consequence of this structural change, from three-fold in phase I and II to five-fold in phase III, is a weakening of Ge-S bond strength (or order) in phase III and thereby a stronger pressure shift of the symmetric Ge-S stretching Ag mode, as observed in Fig. 2.

Figure 7 shows the pressure-volume compression curves of GeS polymorphs and the bulk moduli B_0 calculated based on the 3rd order Birch-Murnaghan equation of state (BM-EOS). The calculated BM-EOS parameters are: $B_0=39.8(3.0)$ GPa and $B_0'=4.2(2.2)$ for phase I; $B_0=71.3(3.1)$ GPa and $B_0'=4.7(3.3)$ for phase II; and $B_0=121.1(3.9)$ GPa and $B_0'=3.4(1.7)$ for phase III. The estimated volume at ambient pressure are: $V_0 = 164.6 \text{ \AA}^3$ for phase I, 152.0 \AA^3 for phase II, and 137.0 \AA^3 for phase III. Note that the bulk modulus of phase III is substantially greater than that of phase II, presumably because of stronger bonding between the layers or a more extended nature of phase III.

Note in Fig. 7 that the phase I→II and II→III transitions are associated with small volume drops of ~3.5 % at 9 GPa and 1.4% at 32 GPa, respectively. This is typical in a way that similar volume changes were previously observed in other group IV mono chalcogenides [11,12,19]. However, it is also important to recognize that the present transitions in GeS are not sharp, but occur over a broad pressure range as illustrated in Fig. 7. Based on the x-ray refinement, it is apparent that a small amount of phase II coexists with phase III even at 49 GPa. The diffraction pattern obtained at pressures between 9 and 19 GPa can also be described by the crystal structure of phase I. In this pressure range, the measured volume difference gradually decreases from 3.5% at 9 GPa to zero at 19 GPa. Similarly so is for phase II and III, no volume difference at 40 GPa. Therefore, these results seem to indicate a sluggish nature of both I-II and II-III transitions, or an intermediate nature of phase II arising from shear-induced structural distortions of double-layered phase I.

Figure 8 plots the pressure-dependent structure parameters and inter- and intra-layer Ge-S bond lengths, showing strong anisotropic behaviors. For clarity, the lattice parameters of phase III were transformed in the (b, c, a) order to plot together with phase I and II and the longest parameter a is plotted with $a/3$ in the plot. Clearly, the c -axis along the puckered layer is more compressible than the a -axis normal to the weakly bonded double layers, in all three phases. However, the effect of such an anisotropic compression becomes weaker in phase III; for instance, the anisotropic compression ratio between the a - and c -axes is ~50% in phase I and ~30% in phase III. The change of the monoclinic lattice angle β is initially minute but becomes significant above 20 GPa.

While maintaining strong anisotropic compression in phase III, the intralayer average Ge-S distance is relatively small with pressure. Yet, the average interlayer Ge...S distance decreases linearly with increasing pressure, which makes the interlayer Ge..S comparable to intralayer Ge-S distances at 49 GPa. This leads to a network structure at this pressure by the formation of new Ge-S bonds and increasing the coordination number to five.

C. Resistance measurements

In addition to the structural phase transitions, GeS also undergoes an insulator-to-metal transition at ~15-20 GPa (Fig. 9). The measured resistance of GeS rapidly decreases by seven orders in magnitude to less than 10 Ω at 20 GPa -- a typical value for metals in this DAC four-probe configuration [25,28]. The metallization of GeS is also apparent from a distinctive color change of the sample from opaque black to reflective gold, as shown in the inset. Note that the reflectivity of the sample at 15 GPa is comparable to that of Pt electrodes, yet it is heterogeneous as if indicating a gradual insulator-metal transition of phase II. Note on a kink at 12 GPa of the pressure-resistance curve, measured during both loading and unloading pressures. This seems to signify the onset of metallization in phase II. However, because of the sluggish structural transition, the resistance value continues to decrease and reaches a steady value only at ~20 GPa, where all phase I is converted to phase II. During decompression, following a hysteresis cycle, the resistance of the sample returns to its original value.

To further confirm the metallic state, we have also examined the resistance at low temperatures. The results are plotted in Fig. 10, indicating a gradual transition from a semi-conductor to a metal. For example, a monotonic decrease in resistance with decreasing temperature above 16 GPa clearly underscores a metallic behavior, whereas the resistance increase at low temperatures in the pressure range between 3 and 11 GPa signifies a limited electron mobility of semiconductors. The $1/T$ dependence of resistance observed at 16 GPa in Fig. 10(b) further suggests the metallic behavior. On the other hand, the electric conductivity at low pressures show a considerable deviation from the $1/T$ dependence, as noted below $\sim 153\text{K}$ at 3.5 GPa (i.e $1000/T > \sim 6.5$ noted by a small arrow in Fig. 10(b)). This is expected for a semiconductor, as its transport process does not follow a single thermal activation process. The metallic nature of GeS retains across the phase II-III transition to 46 GPa the highest pressure studied.

DISCUSSION

The present results show evidence for two structural phase transitions, from a low pressure $Pnma$ (or $Pbnm$, B16) to a high-pressure $Cmcm$, B33) structure via a distorted monoclinic $P2_1/m$ structure over a wide-range of pressure. These transitions arise from anisotropic compression and enhanced shears in the layered structures. In turn, the transitions manifest an increase in the nearest coordination numbers for Ge and S atoms from three in phase I and II to five in phase III. This coordination increase reflects the formation of covalent bonds between the double layers of phase III, which makes it an

extended network of densely packed double layers, analogous to a distorted rock salt (B1) structure predicted previously [14,16]. The monoclinic $P2_1/m$ structure of phase II, on the other hand, can be considered as an intermediate structure arising in the transition pathway from the B16 (phase I) to B33 (phase III) structure. The phase I-to-II transition can then be described by the group-sub group relationship between $Pnma$ and $P2_1/m$ – the relationship often found in the shear-driven displacive transition.

These structural phase transitions are consistent with the observed Raman spectral changes. The emergence of a new feature on the high frequency side of the A_g mode above 9 GPa, for example, is at the onset of the phase I-to-II transition. The appearance of another new peak at $\sim 370\text{ cm}^{-1}$ above 28 GPa seems to correlate to the II-to-III transition at ~ 32 GPa, albeit a small pressure hysteresis in the transition. Importantly, the faster pressure-shift of the A_g mode at 270 cm^{-1} above 9 GPa reflects weakening of intralayer Ge-S bond strength in response to enhanced interlayer Ge..S interactions, which eventually lead to the five-fold coordinated pyramidal structure in phase III.

The present study depicts the onset of metallization at ~ 12 GPa at ambient temperature, although the resistance value continues to decrease until pressure reaches to 20 GPa. We attribute this to the sluggish I \rightarrow II transition occurring over the pressure range of 9-19 GPa. On the other hand, it is not apparent if the metallization occurs at the onset of structural phase transition based on the small pressure difference observed between the x-ray and Raman data (at 9 GPa) and the resistance measurements (12 GPa). Regardless, the metallization occurs gradually over the pressure range 12 to 20 GPa, primarily because of the pressure-induced band broadening in phase II. For comparison,

the bandgap of GeS is ~ 1.5 eV at ambient pressure [29], which was predicted to close at 16 GPa based on the *Cmcm* structure [21].

In conclusion, the structural phase transitions in dense GeS occurs displacively from low-pressure phase I (*Pnma*, B16) to high-pressure phase III (*Cmcm*, B33) via intermediate phase II (*P2₁/m*) over a broad pressure range from 9 GPa to well over 36 GPa. These transitions are accompanied by an increase of the nearest neighbor coordination number of Ge and S from three in phase I and II to five in phase III, resulting in an extended 3D network of closely packed layer structures in phase III. We suggest an anisotropic-compression enhanced shear mechanism in these double layer structures to be responsible for the observed structural phase transitions. We also found the metallization of GeS in the pressure regime of phase II (*P2₁/m*), as previously predicted [21]. The effect of pressure medium in the proposed shear-induced phase transition is important but difficult to quantify, especially using powder samples. Therefore, future study should emphasize on similar studies using single crystal GeS in various pressure media.

ACKNOWLEDGEMENTS

The present study has been performed in support of NSF-DMR (Grant No. 1203834) and DTRA (HDTRA1-12-01-0020). The x-ray work was performed at the HPCAT in support of CDAC. HPCAT operations are supported by DOE-NNSA (DE-

NA0001974) and DOE-BES (DE-FG02-99ER45775). We thank Dr. G. Bostad for his assistance in synchrotron x-ray experiments at the APS.

REFERENCES

1. R. B. Shalvoy, G. B. Fisher, and P. J. Stiles, *Phys. Rev. B* **15**, 2021 (1977).
2. D. Trbojevic, P. M. Nikolic, B. Perovic, and V. Cekic, *Appl. Phys. Lett.* **38**, 362 (1981).
3. B. Subramanian, C. Sanjeeviraja, and M. Jayachandran, *Mater. Chem. Phys.* **71**, 40 (2001).
4. H. C. Hsueh, M. C. Warren, H. Vass, G. J. Ackland, S. J. Clark, and J. Crain, *Phys. Rev. B* **53**, 14806 (1996).
5. A. Okazaki, *J. Phys. Soc. Jpn.* **13**, 1151 (1958).
6. H. Wiedemeier and H. G. V. Schnering, *Z. Kristallogr.* **148**, 295 (1978).
7. P. B. Littlewood, *J. Phys. C* **13**, 4855 (1980)
8. T. Chattopadhyay, A. Werner, and H. G. von Schnering, *High Pressure in Science and Technology*, edited by C. Homan, R. K. MacCrone, and E. Whalley, MRS Symposia Proc. No. 22 Materials Research Society, Pittsburgh, p 83 (1984).
9. K. L. Bhatia, G. Parthasarathy, D. P. Gosain, and E. S. R. Gopal, *Phys. Rev. B* **33**, 1492 (1986).
10. M. Parenteau and C. Carlone, *Phys. Rev. B* **41**, 5227 (1990).
11. J. M. Leger and A. M. Redon; *J. Phys.: Cond. Matter* **2**, 5655 (1990).

12. L. Ehm, K. Knorr, P. Dera, A. Krimmel, P. Bouvier, and M. Mezouar, *J. Phys.: Cond. Matter* **16**, 3545 (2004).
13. H. C. Hsueh, H. Vass, S. J. Clark, G. J. Ackland, and J. Crain, *Phys. Rev. B* **51**, 16750 (1995).
14. P. Toledano, K. Knorr, L. Ehm, and W. Depmeier, *Phys. Rev. B* **67**, 144106 (2003).
15. G.-S. Do, J. Kim, S.-H. Jhi, C.-H. Park, S. G. Louie, and M.L. Cohen, *Phys. Rev. B* **82**, 054121 (2010).
16. M. J. Buerger, in *Phase transformation in Solids*, edited by R. Smoluchowski, J. E. Mayers, and W. A. Weyl (Wiley, New York, 1951), p.183.
17. L. G. Khvostantzev, V. A. Sidorov, L. E. Shelimova, and N. Kh. Abrikosov, *Phys. Stat. Sol. A* **74**, 185 (1982).
18. A. F. Wells, *Structural Inorganic Chemistry*, 4th ed. (Clarendon, Oxford, 1975).
19. A. Onodera, I. Sakamoto, Y. Fujii, N. Mori, and S. Sugai, *Phys. Rev. B* **56**, 7935 (1997)
20. L. Yu, A. Degiovanni, P. A. Thiry, J. Ghijsen, R. Caudano, and Ph. Lambin, *Phys. Rev. B* **47**, 16222 (1993)
21. M. Durandurdu, *Phys. Rev. B* **72**, 144106 (2005)

22. A. P. Hammersle Cambriay, S. O. Svensson, M. Hanfland, A. N. Fitch, and D Häusermann, *High Press. Res.* **14**, 235 (1996)
23. A. C. Larson and R. B. Von Dreele, *Los Alamos National Laboratory Report LAUR* 86 (2000).
24. B. H. Toby, *J. Appl. Cryst.* **34**, 210-213 (2001).
25. L. J. van der Pauw, *Philips Research Reports* **13**, 1 (1958)
26. J.D. Wiley, W.J. Buckel and R.L. Schmidt, *Phys. Rev. B* **13**, 2489 (1976).
27. G. Burns and A.M. Glazer, *Space Groups for Solid State Scientists* (Academic, New York, 1978).
28. R. P. Dias, C. S. Yoo, et al., *Proc. Nat. Acad. Sci.* **110**, 11720 (2013).
29. L. Makinistianm and E. A. Albanesi, *Phys. Rev. B* **74**, 45206 (2006).

Table 1. Structure information of GeS in pressure. Lattice parameters and atomic positions were refined by the Rietveld refinement method.

GeS polymorphs	Phase I at 5 GPa	Phase II at 16 GPa	Phase III at 49 GPa
Structure	<i>Pnma</i>	<i>P2₁/m</i>	<i>Cmcm</i>
a (Å)	10.068	9.628	3.624
b (Å)	3.605	3.506	9.030
c (Å)	4.055	3.780	3.367
β (γ) ($^\circ$)	90	90.10	90
Ge1	(0.386,0.25,0.088)	(0.620,0.25,0.618)	(0.0, 0.859, 0.25)
Ge2		(0.120,0.25,0.882)	
S1	(0.149,0.25,-0.020)	(0.354,0.25,0.008)	(0.0, 0.592, 0.25)
S2		(0.854,0.25,0.501)	
Z	4	4	4
Volume (Å ³)	147.18	128.25	110.18
ρ (g/cm ³)	4.723	5.420	6.309
Ge-S1, intralayer (Å)	2.429	2.286	2.512
Ge-S2, intralayer (Å)	2.426	2.293	2.415
Ge...S, interlayer (Å)	3.509	2.945	2.773
Ge-S-Ge; S-Ge-S ($^\circ$)	95.82	100.092	92.34
Ge-S2-Ge ($^\circ$)	105.12	103.35	79.91
Interlayer distance	2.295	2.312	1.6596
Coordination number	3	3	5

FIGURE CAPTIONS

Fig. 1 Pressure-induced Raman changes of germanium sulfide during pressure loading (a) and unloading (b). The spectra shows splitting in Raman spectra in the 260 cm^{-1} region (A_g mode) and new rather broad peak appear at $\sim 331\text{ cm}^{-1}$ above 28 GPa indicating a structural phase transition. The unloading spectra show the reversibility of the pressure-induced spectral changes.

Fig. 2 (a) Pressure-induced shifts of the Raman peaks (A_g and B_g modes) of GeS, clearly indicating the splitting of the A_g mode and the emergence of new peak above 28 GPa. The close and open symbols signify the data taken during the pressure uploading and downloading, respectively. (b) The spectral deconvolution of Raman spectra of GeS polymorphs, used to find the reported peak positions in Fig. 2a from the data in Fig. 1.

Fig.3 Angle resolved x-ray diffraction patterns of GeS to 49 GPa. The asterisk ‘*’ marked at ambient-pressure data indicates a spurious feature from impurity.

Fig. 4 Pressure dependent shifts of observed interplanar d-spacings of GeS to 49 GPa. Vertical lines denote the onset pressures of structural phase transitions. The inset shows the 2D diffraction images of GeS polymorphs to show evidence for textured lattice and preferred orientation.

Fig. 5 Observed (dotted ‘x’), calculated (black line), and difference (red line) diffraction data at 5 GPa for phase I in $Pnma$, 16 GPa for phase II in $P2_1/m$, and 49 GPa for phase III in $Cmcm$. The blue tick marks indicate (hkl) reflections of corresponding space groups.

Green tick mark at 49 GPa represents the reflection from monoclinic cell as a minor phase. Asterisk ‘*’ marked at 2 GPa indicates impurity.

Fig. 6 Constructed crystal models of various phases of GeS. (a) Orthorhombic structure in $Pnma$ of phase I, (b) monoclinic structure in $P2_1/m$ of phase II, and (c) orthorhombic structure in $Cmcm$ of phase III. All presented values are based on the refined structures. Solid box presents a unit cell. Dotted line presented nearest neighboring intermolecular Ge-S distance.

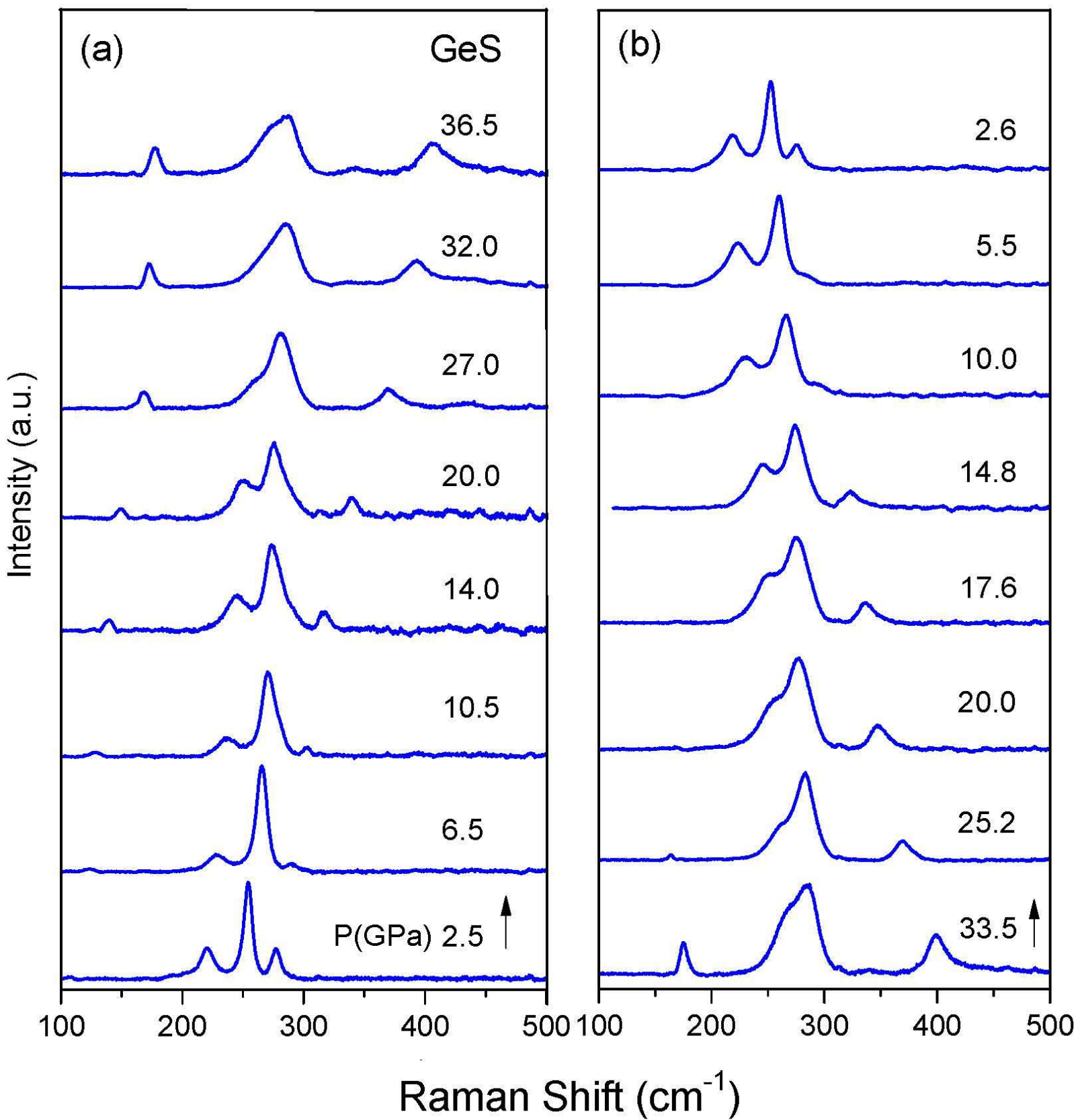
Fig. 7 The pressure-volume compression curve of GeS polymorphs, showing together with 3rd-order Birch-Murnaghan equation of state fits (solid lines). The long vertical dotted lines at 9 and 32 GPa signify the structural phase transitions, respectively, from phase I to II and phase II to III. The short vertical dash-dot line at 18 GPa signifies the electronic insulator-metal transition of phase II.

Fig. 8 (a) Pressure dependence changes of lattice parameters and angles. Cell parameters of phase III were transformed to the order with (b, c, a). Vertical dot-dashed lines at 9 GPa and 36 GPa indicate the onsets of phase transitions. (b) Pressure dependent changes of the nearest interlayer Ge..S distance and two nearest intralayer Ge-S bond distances.

Fig. 9 The pressure dependence of the electrical resistance of GeS at room temperature, showing a sharp decrease (seven orders in magnitude) of the resistance at 18 GPa, indicating the electronic transition from an insulator to a metal. An anomalous kink at 12 GPa is likely due to the inception of metallic phase II. The inset shows the sample becomes shiny around 15GPa providing the visual evidence for the metallization. The

close and open symbols denote the data taken during the pressure uploading and downloading, respectively.

Fig. 10(a) The temperature-dependent electrical resistance of GeS at 3, 6, 11 GPa on a logarithmic scale, showing a transition from semiconductor to semi-metal, and 16, 21, 46 GPa showing the clear metallic behavior. (b) The $\ln(\rho)$ against $1000/T$ (Arrhenius plot), showing the linearity indication by red lines.



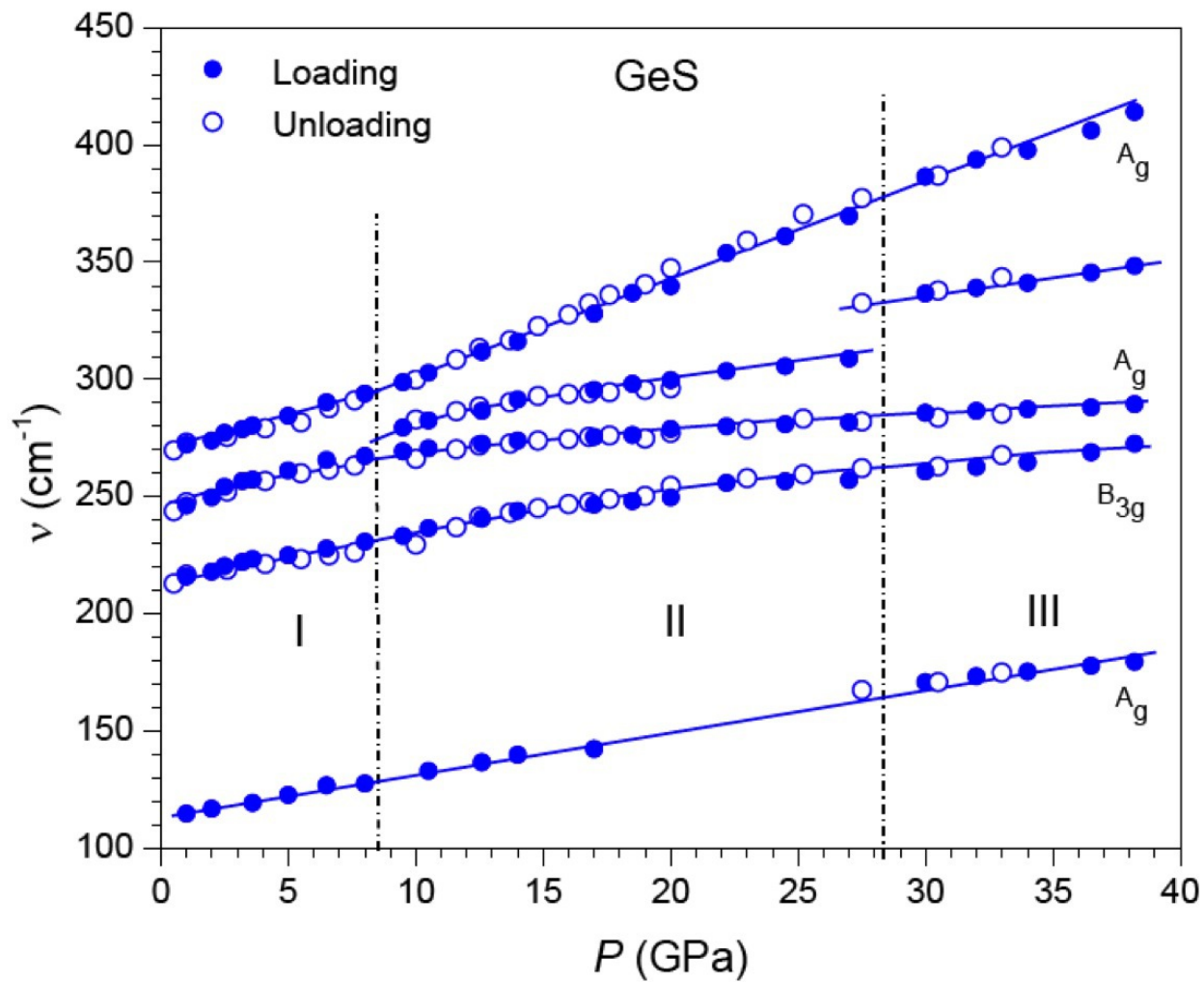


Fig. 2

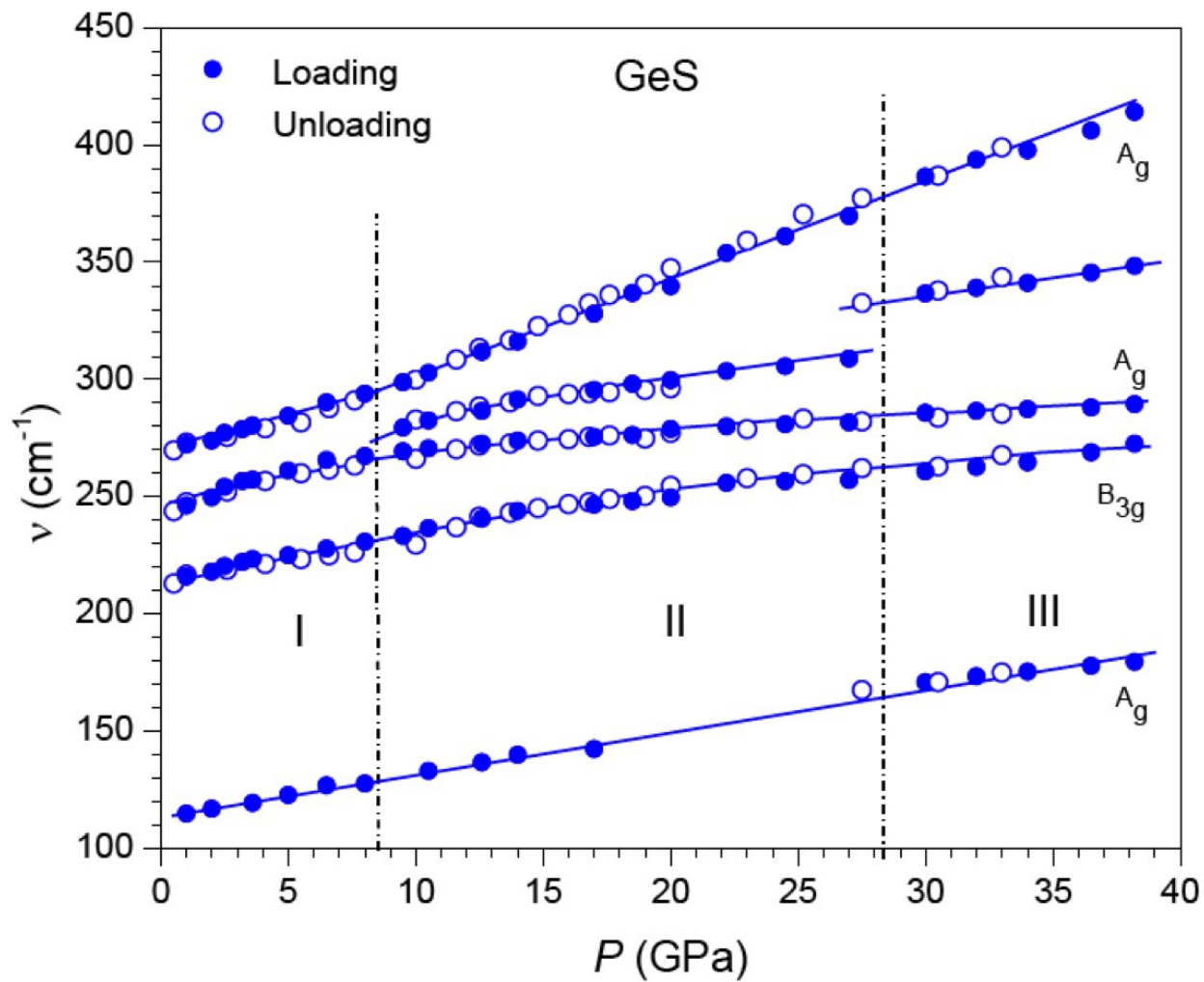
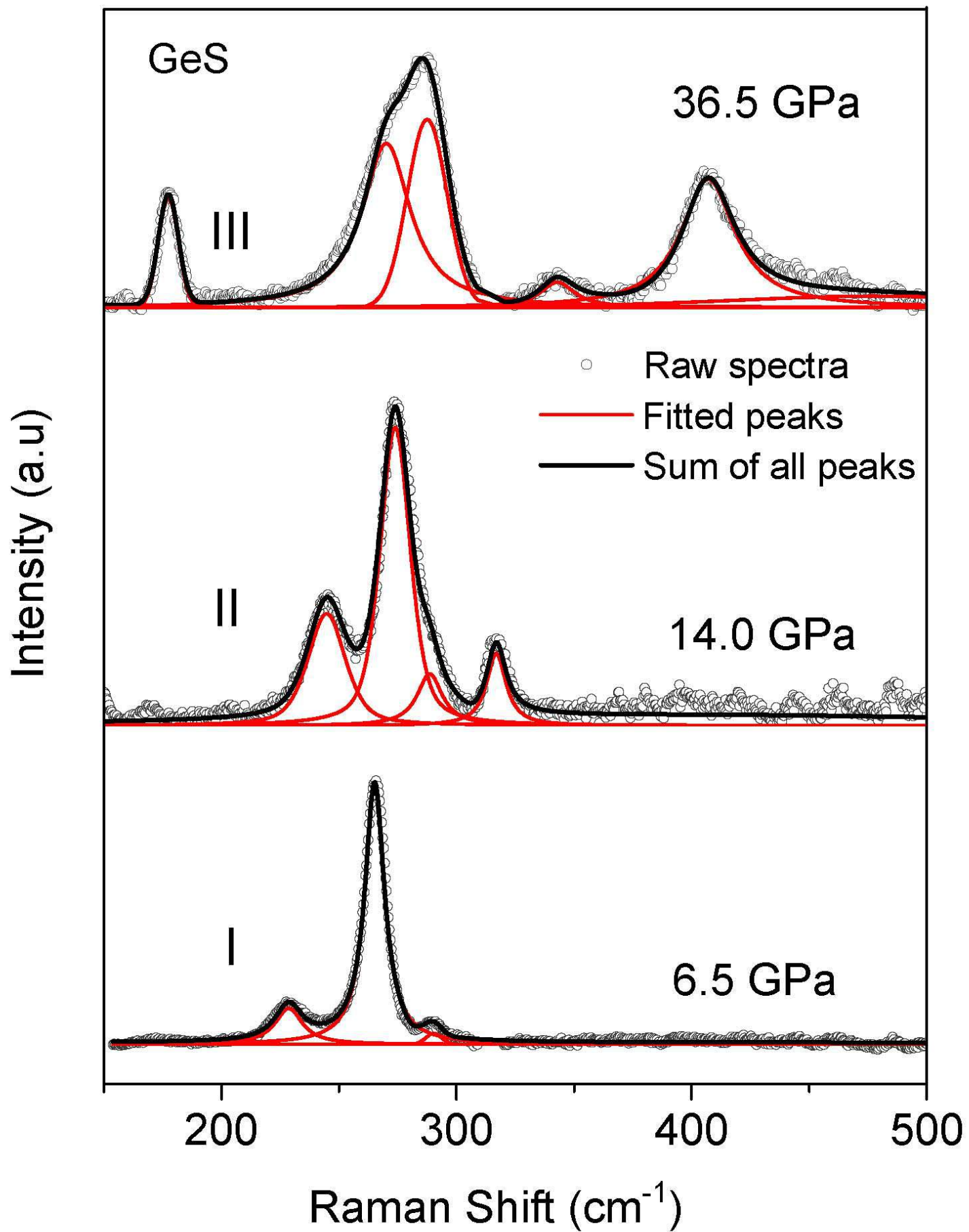


Fig. 2



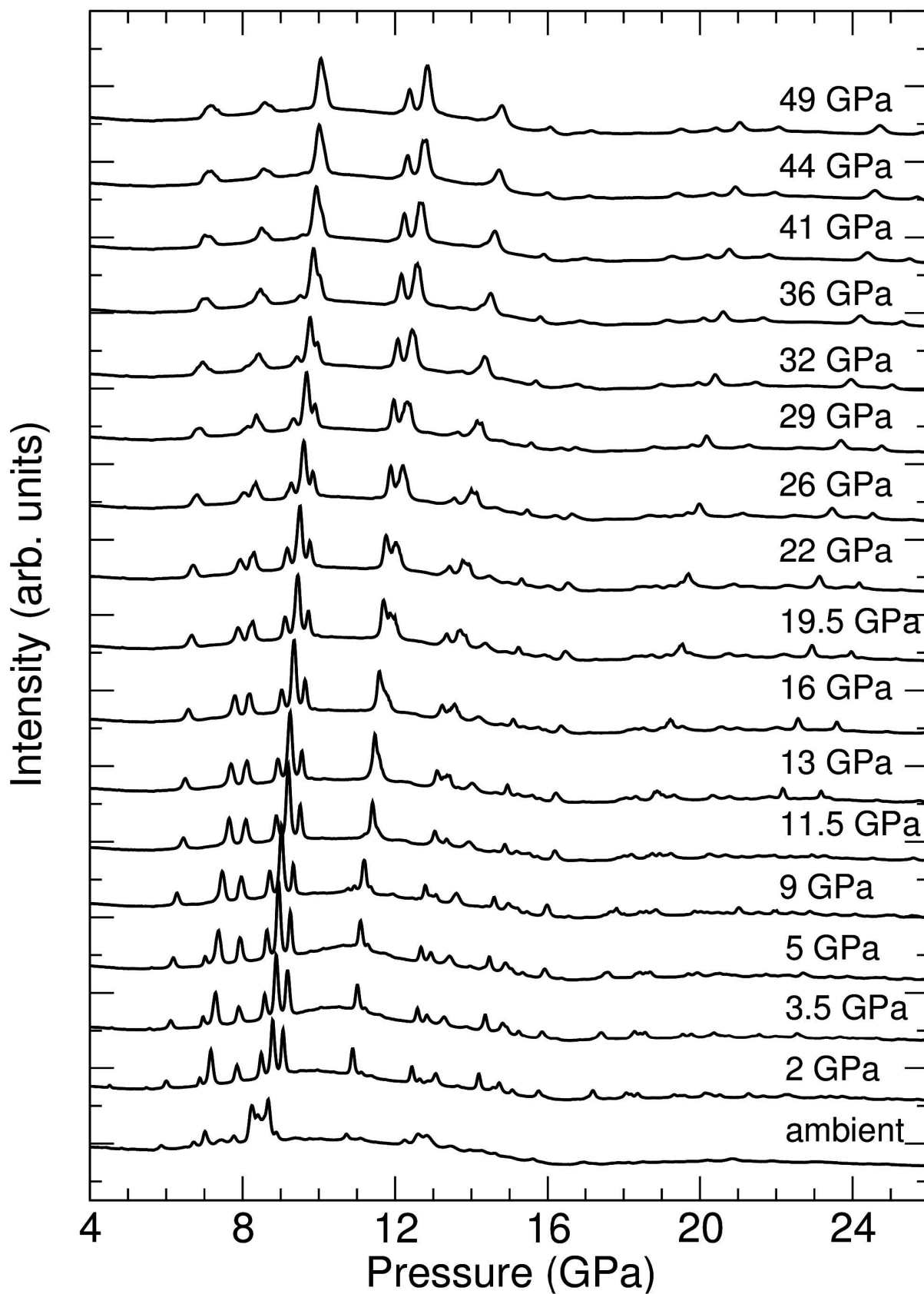
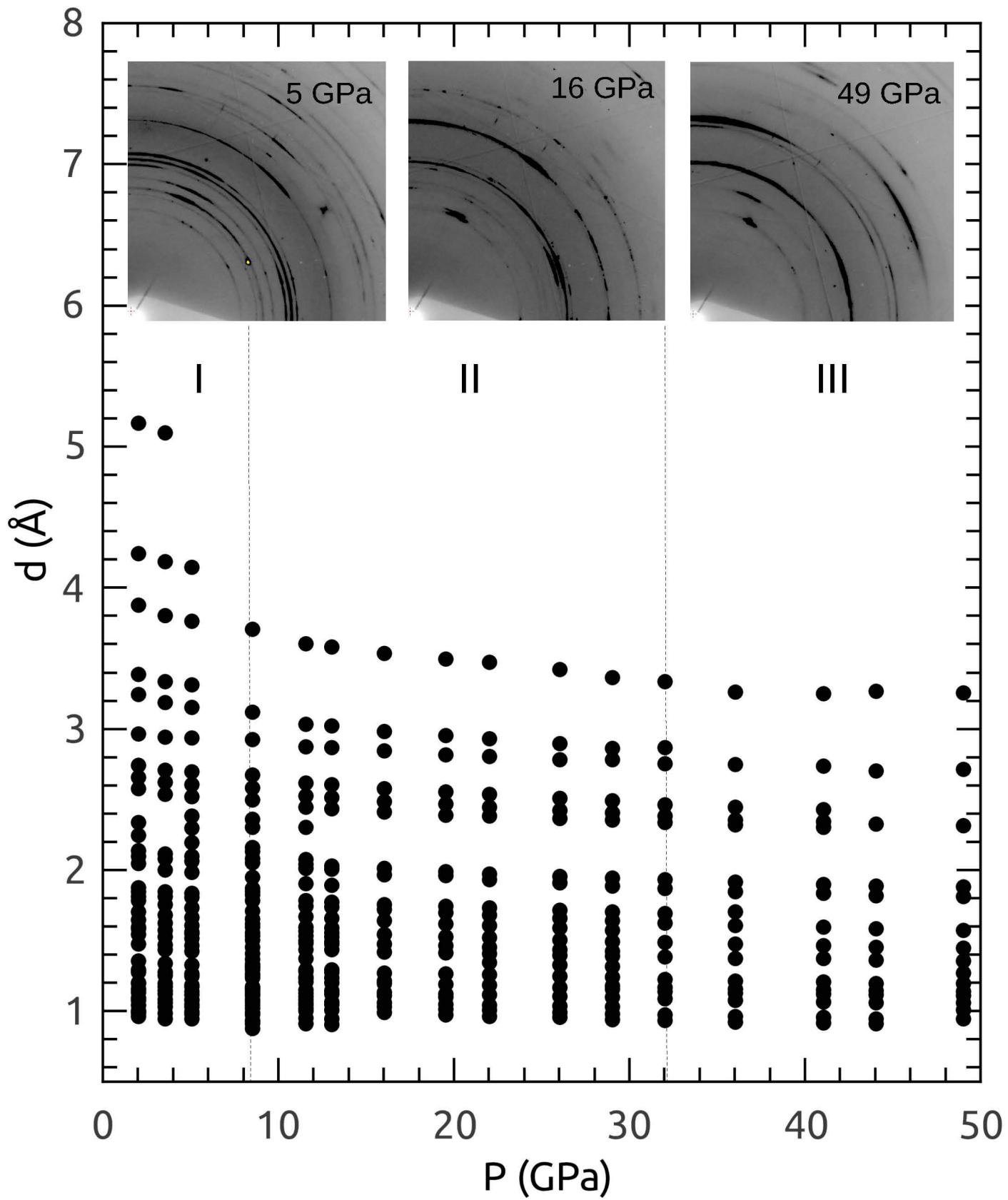


Fig. 3



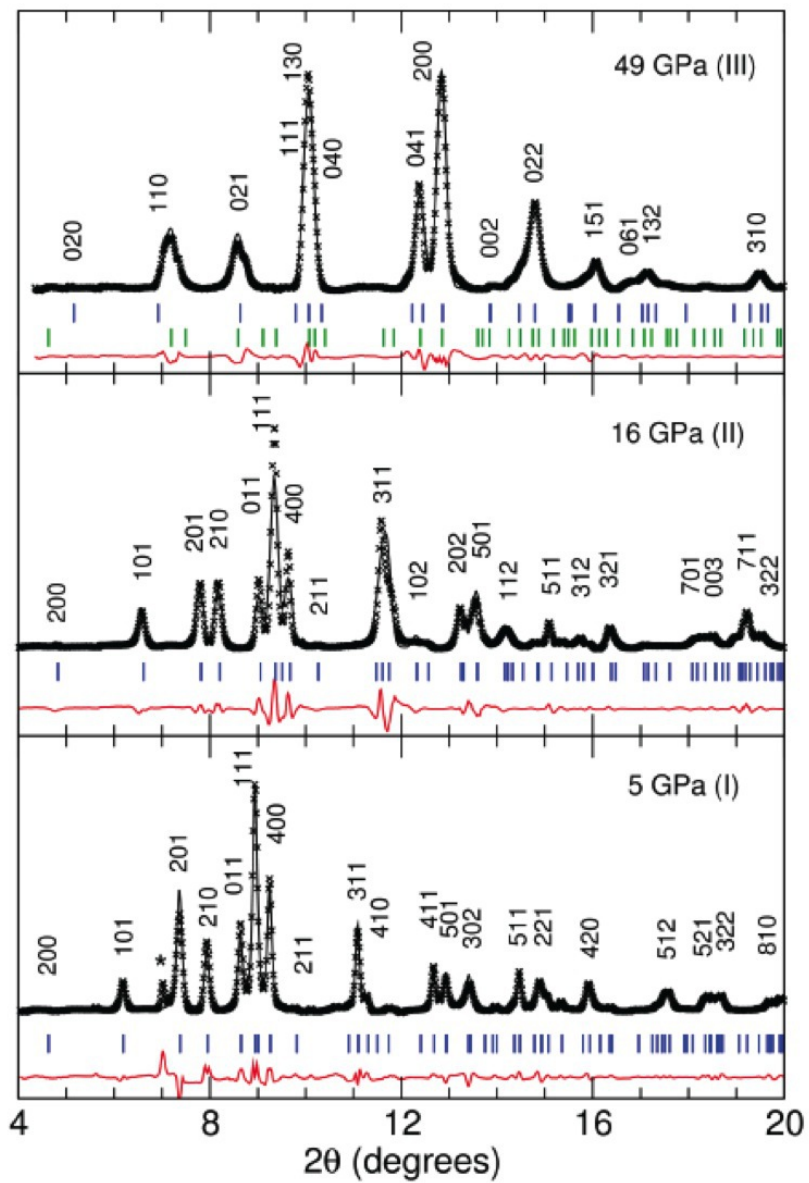
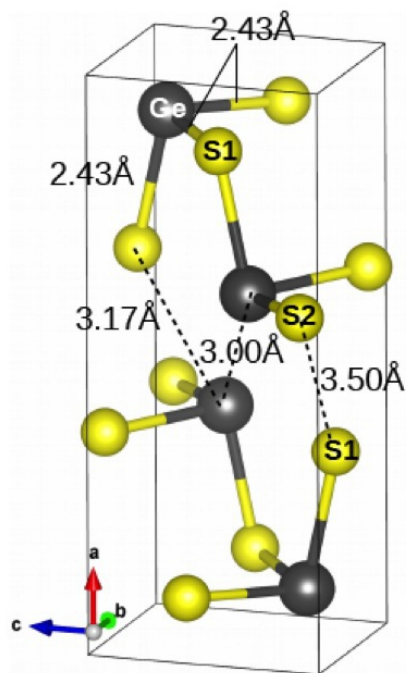
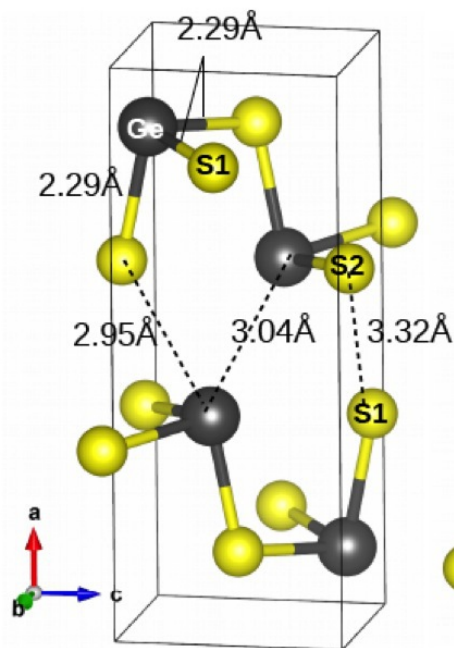


Fig. 5

(a) I (5 GPa)



(b) II (16 GPa)



(c) III (49 GPa)

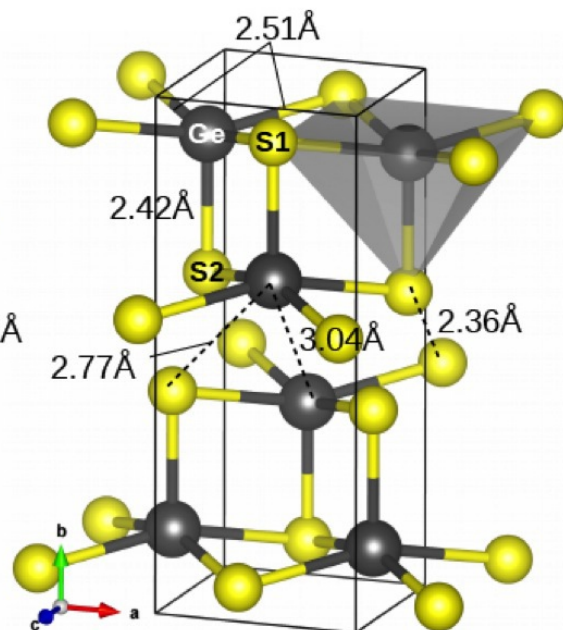


Fig. 6

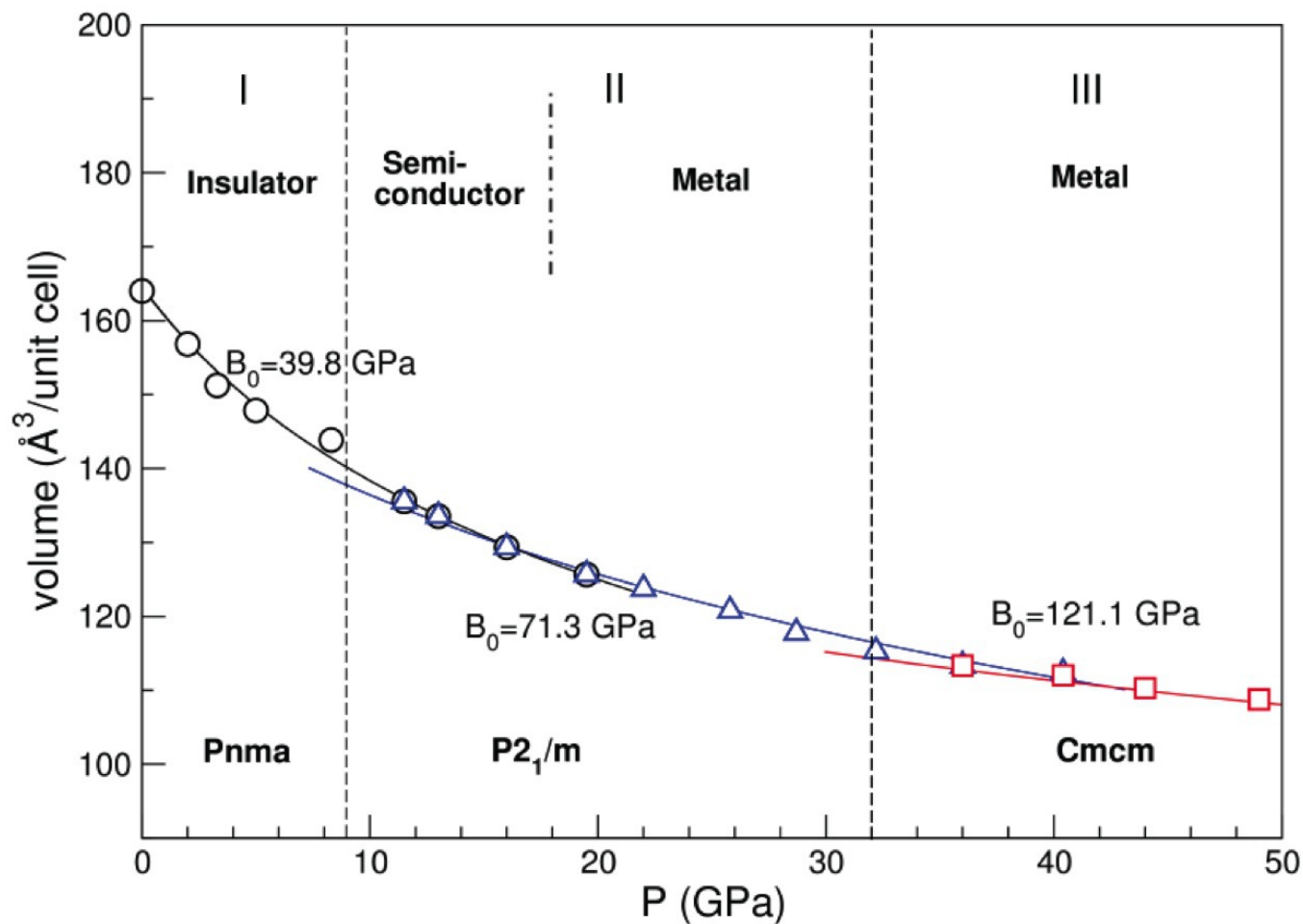


Fig. 7

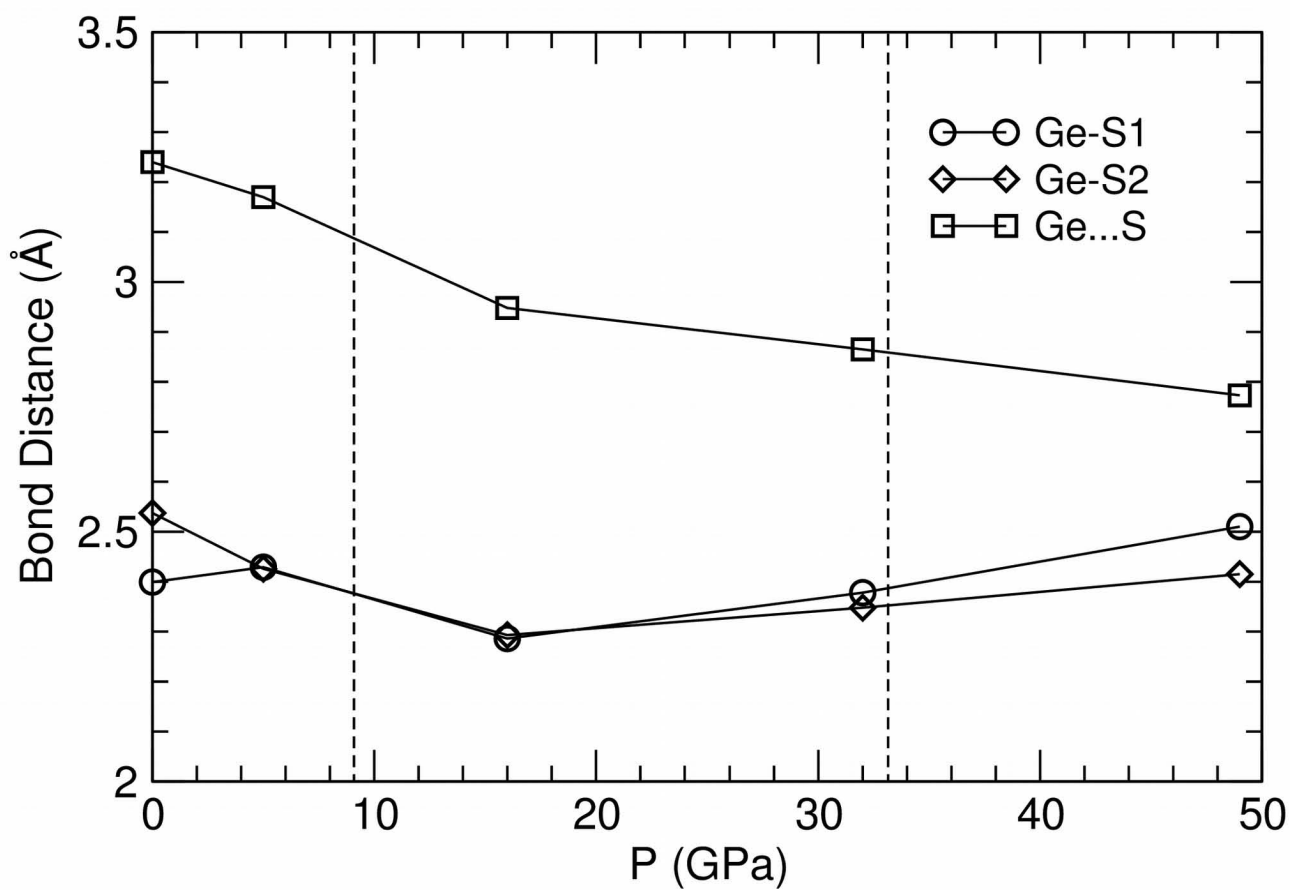
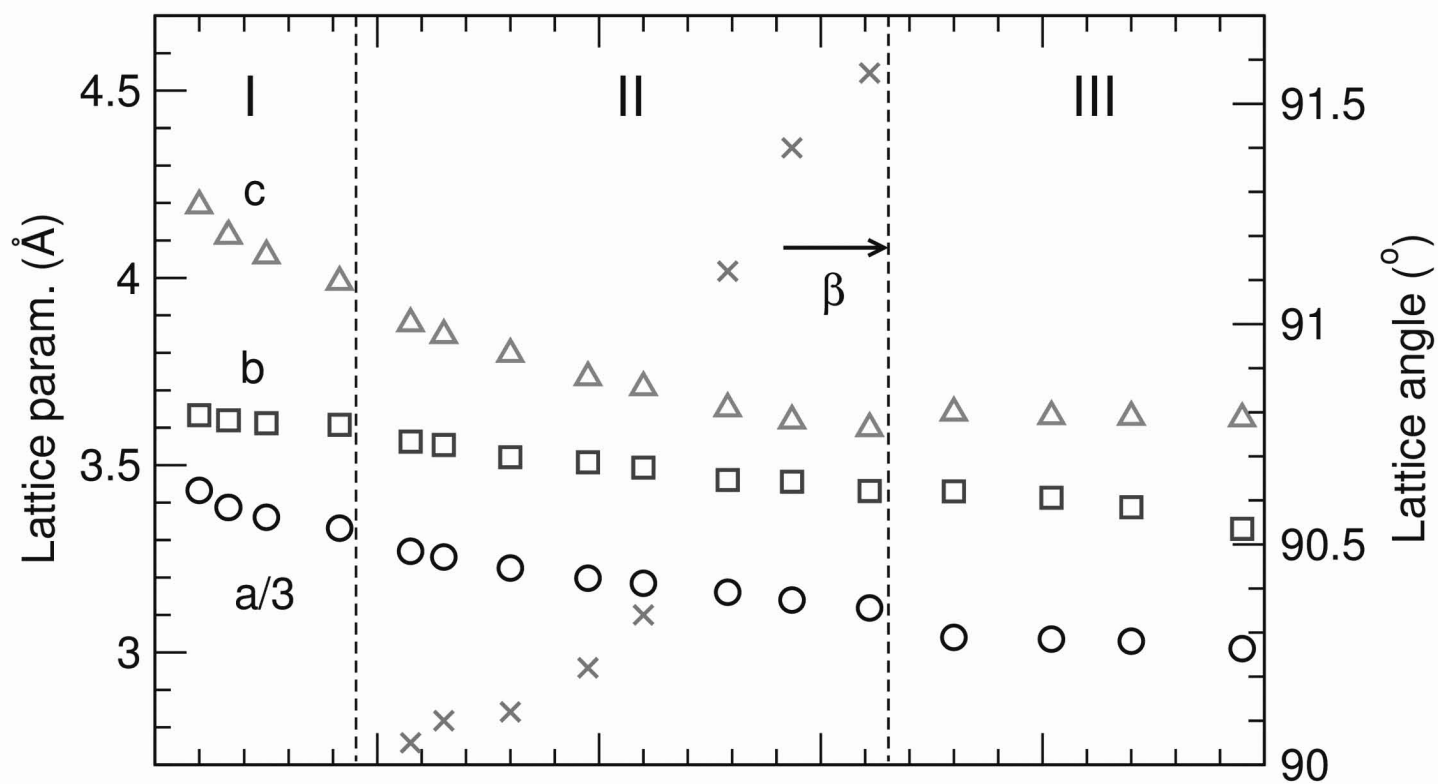


Fig. 8

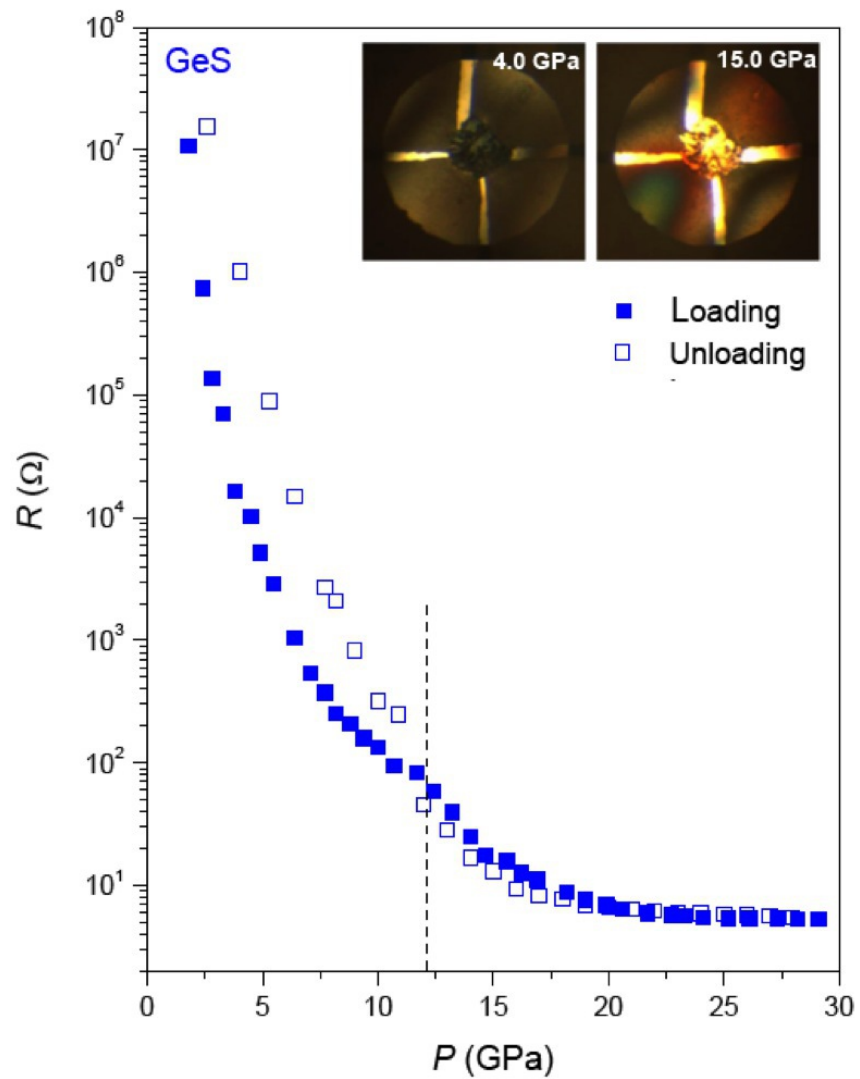


Fig. 9

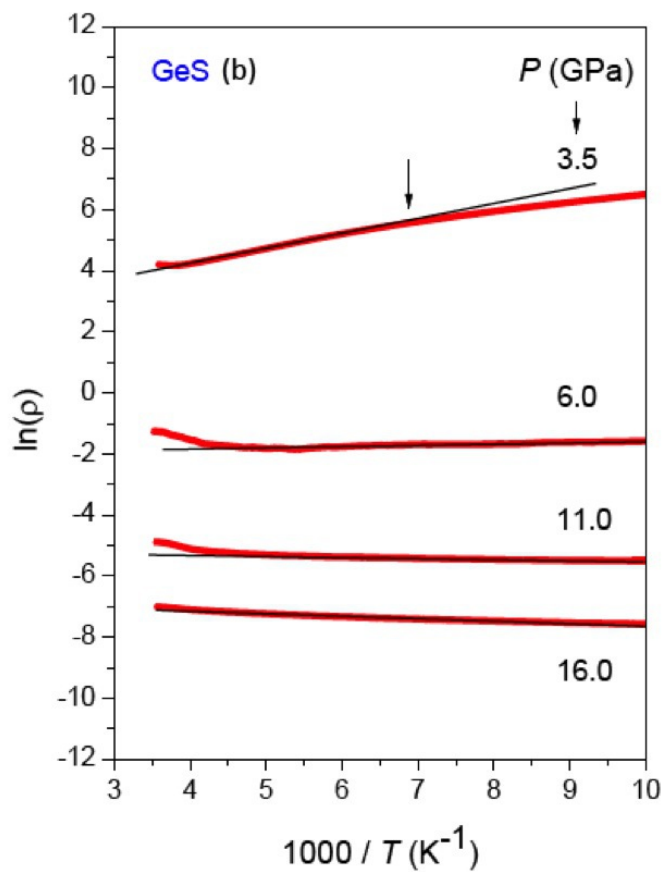
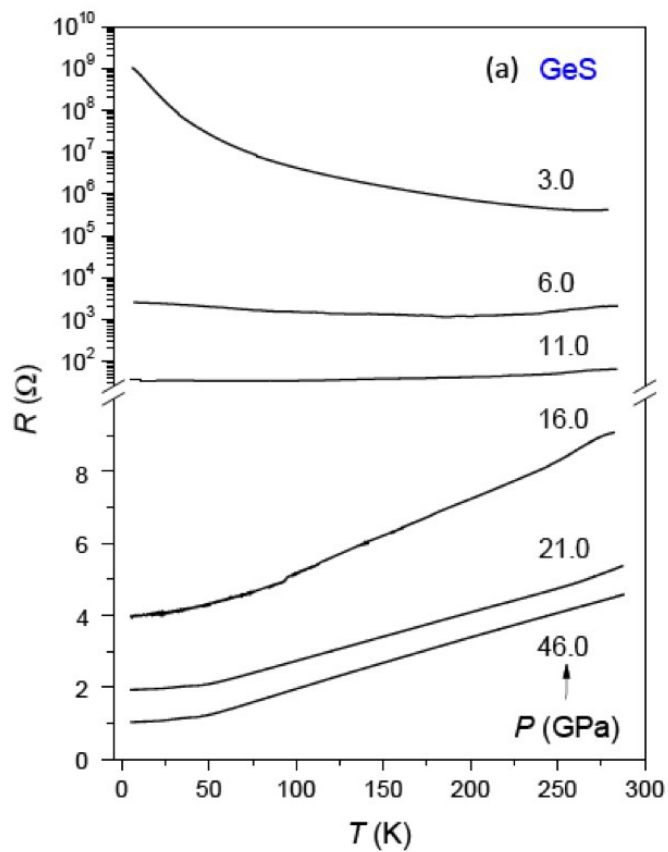


Fig. 10